DUAL-USE STRAIN SENSORS FOR SIMULTANEOUS STRAIN MEASUREMENT AND ACOUSTIC SOURCE LOCATION

JASON ANDREW SMITH

Thesis submitted to the faculty of the Virginia Polytechnic Institute and State University in partial fulfillment of the requirements for the degree of

Master of Science

In

Mechanical Engineering

Wing F. Ng, Chair

Alfred L. Wicks

Robert L. West

July 29, 2024

Blacksburg, VA

Keywords: Acoustic Emission, NDE, SHM, Piezoresistive, Quasi-Static Fracture, Source Location, CT Specimen

DUAL-USE STRAIN SENSORS FOR SIMULTANEOUS STRAIN MEASUREMENT AND ACOUSTIC SOURCE LOCATION

JASON ANDREW SMITH

Abstract

The use of metal strain gauges and ultrasonic transducers have long been studied in the field of Nondestructive Evaluation (NDE) as a part of structural health monitoring (SHM). Strain gauges use electrical resistance to monitor strains during the loading of a component. Ultrasonic transducers are piezo devices that use a crystal-like sensing element with very low excitation energy that can monitor small strains such as acoustic emissions (AEs). These types of devices have been used to locate the sources of AEs from artificial sources, such as Hsu-Nielsen pencil lead break (PLB) tests, or natural sources such as quasi-static fracture or crack propagation. This type of evaluation has significant advantages over other types of damage inspections such as liquid die penetrant, Blue Light, Eddy Current, or X-ray inspections where visual inspections, large defects, and high levels of user experience are required.

The ultrathin silicon membrane (USM) sensor developed by NanoSonic Inc. is a piezoresistive sensor, incorporating the best aspects of a conventional strain gauge and ultrasonic transducer. The sensor can measure both the strain of a component, as well as any acoustic emission that is emitted on the component. To the author's knowledge this is the only sensor capable of simultaneous measurement of these two data types. This paper presents the sensor's ability to be used for quasi-static fracture monitoring. The sensor is first compared to commercial ultrasonic transducers in an unloaded pencil lead break (PLB) test for determining the ability in measuring lamb waves for source location estimation. The NanoSonic USM sensor is further compared to commercial strain gauges and ultrasonic transducers during a PLB test under a tensile load where it is demonstrated the USM sensor yields similar measurements to both commercial sensors. The final test was a quasi-static fracture test, where the NanoSonic USM sensor was able to detect substantially lower energy AEs than the previous test and record the strain history during fracture. This duality of the USM sensor demonstrates an inherent usefulness to NDE and SHM fields. The sensor offers sensing capabilities comparable to commercially available sensors in a smaller package, with less power consumption, at a lower cost.

DUAL-USE STRAIN SENSORS FOR SIMULTANEOUS STRAIN MEASUREMENT AND ACOUSTIC SOURCE LOCATION

JASON ANDREW SMITH

General Audience Abstract

Nondestructive evaluation (NDE) is a field within structural health monitoring (SHM) that refers to determining any defects within a component that would hinder its performance without modifying its existing condition. This has historically been done by visual inspection by which experienced personnel examine the part for defects. This is inherently flawed as cracking below the surface of a component is common and would not be detected and extensive experience is required to successfully complete this task. Components in hard-to-reach places, with coatings, or that are small also prove challenges to visual inspection. Engineers have developed several new testing methods to combat these flaws. The use of acoustic emission (AE) testing allows sensors, called ultrasonic transducers, to receive and emit sounds at high frequencies to conduct the inspection. This can be done by emitting a sound which is then propagated as a wave along the surface of the component, if the wave hits a defect, it is scattered. A receiving sensor would then receive an unexpected signal, indicating that there is a problem. Furthermore, an array of these sensors can be employed to 'listen' for these surfaces waves that may be emitted during the standard operation of the components. Things like high loads, cracking, and impacts will all be able to be detected. The use of an array of sensors will allow the location of these events.

This paper will discuss a new type of sensor, an ultrathin silicon membrane (USM) sensor developed by NanoSonic Inc. This type of sensor can detect high frequencies similar to an ultrasonic transducer, as well as measure large loads that would deform the part, resulting in an event known as strain. The novelty of the NanoSonic USM sensor is its ability to monitor both pieces of information simultaneously, which is believed to be the first to do so in the field. The ability to obtain information on strain and locations of acoustic events within a component during standard operation would be a valuable prospect for the aerospace, civil, and automotive industries.

Acknowledgement

First, I want to thank my whole family, specifically, my mother, Karen Smith, and my father, Thomas Smith for their unwavering love, support, and encouragement before, during, and after my time at Virginia Tech as a part of this program. An additional thank you to my Uncle Jeff and Uncle Walter for their encouragement and guidance while starting my education and career as an engineer. My greatest thanks to my Aunt Linda, and Grandfather John, for helping me finish this journey from above. Finally, I want to thank my dearest friends Daniel, Patrick, Nick, Nick, Sam, and Garek for their utmost support during this journey.

Next, I want to acknowledge and thank my advisor Dr. Ng, for the opportunity to work with him and participate in his research which heightened my professional skills. I would like to further thank Dr. Ng, and my committee Dr. West, and Dr. Wicks for their guidance and imparting their engineering wisdom throughout this research.

I want to express my utmost gratitude to this University for providing an exceptional five years. I will look fondly upon this time as a chapter of growth, friendship, leadership, and perseverance that will leave a lasting impact on my life. The support from the faculty as an undergraduate and graduate student has allowed me to learn and apply topics that a younger version of myself would have only dreamed of.

Finally, I want to thank the team at NanoSonic Inc. Dr. Hang Ruan, Josh Deem, Albrey de Clerck, and Noah Jones. Their engineering expertise and endless support for this project has been instrumental in the developments that will be discussed in this paper. My time with the sensors team has certainly made me a better engineer and researcher. There were truly no bad days when working with them.

Table of Contents

Table of Figures

Table of Tables

DUAL-USE STRAIN SENSORS FOR SIMULTANEOUS STRAIN MEASUREMENT AND ACOUSTIC SOURCE LOCATION

Jason Smith[1], Albrey de Clerck[2], Noah Jones[2], Josh Deem[2], Hang Ruan[1,2]*, Wing Ng[1]*

[1]Department of Mechanical Engineering, Virginia Tech; Blacksburg, VA 24061
[2]NanoSonic, Inc.; 158 Wheatland Drive, Pembroke, VA 24136

Nomenclature

E	Modulus of Elasticity
G	Shear Modulus
ν	Poison's Ratio
ρ	Density
ω	Wave frequency (rad/s)
c_p	Wave phase velocity
c_L	Longitudinal Wave Velocity
c_T	Transverse Wave Velocity
K	Stress intensity factor
α	Thickness ratio
P	Force
t	CT Specimen Thickness
b	CT Specimen Width

1. Introduction

The field of structural health monitoring (SHM) is a historic cornerstone of many engineering disciplines, establishing a set of governing equations, characteristics, and measurement methods of uniquely loaded components. The ability to provide insight on service life, fatigue, and expected failure methods became critical to the automotive, civil, and aerospace industries in the late 1900s [1]. An additional field would emerge called nondestructive evaluation (NDE) to include methods of determining the overall health of a component without impacting the original functionality during standard operation (infrared and acoustic emission testing) and during maintenance inspections (ultrasonic, liquid penetrant, eddy current) [2]. This paper will focus on acoustic emission testing due to its relation to the Ultrathin Silicon Membrane (USM) developed by NanoSonic Inc. and its ability to be used *in-situ* with source location algorithms.

Acoustic emission (AE) testing was first referenced by Joeseph Kaiser in 1949. His work investigated the correlation of AE events to material properties by conducting various tensile tests and using a microphone to detect AEs [3]. Dunegan and Engle in 1968 would apply AE testing to NDE by monitoring for an emitted surface wave and being able to determine a defect within the part [4]. AE testing can be conducted one of two ways, actively or passively [5].

Active testing requires the emission of a known AE source from an ultrasonic transducer for which an expected return value can be predicted, if the returned value is dissimilar to that of the predicted value, a defect is expected, and further analysis can be conducted. This idea shares many similarities with a 'pinging' method found in sonar.

The active method for using AEs is often referred to as Ultrasonic Testing. Ultrasonic testing has been used in many applications for evaluating different feature types for SHM. Mi *et al*. used ultrasonics to examine crack initiation of rivet holes in aluminum specimens during static and fatigue testing [6]. Arakawa *et al*. used ultrasonics in welded structural steel members to evaluate the occurrence of cracks within the joints due to the brittle nature of welds from carbon build up [7]. Her *et al*. introduced a 3-dimmensional approach to ultrasonic evaluation by determining the depth of a surface crack or defect within a part [8]. Heasler et al. used ultrasonics to inspect for internal cracks at the intergranular level [9]. In the commercial space, the American Society of Testing and Methods (ASTM) developed a standard for ultrasonic testing, ATSM B549 to outline testing procedures and methods.

Passive AE testing uses an emission that is not generated from a sensor and developed naturally by using stress waves when loading a component, or waves formed during fracture, crack initiation or propagation.

Morton discussed this idea by comparing the number of acoustic emissions to crack growth rate and fatigue cycles, where it was found the acoustic emission increased with crack growth rate [10]. Roberts conducted similar studies and found with the number of cycles, the number of AE events also increased [11]. Vanniamparambil used the change in frequency of acoustic emissions to determine the onset of cracking and the severity of the defect [12]. Yu used piezoelectric sensors and CT specimens to locate the tip displacement of a crack [13]. Dris used AE data accompanied with an Extended Kalman Filter (EKF) model to detect and locate the crack tip displacement in an aluminum plate under static loading [14]. Keshtegar used an aluminum compact tension specimen accompanied with acoustic sensors to determine the crack behavior during propagation [15].

A commonality between both AE testing methods is their sensing equipment. The use of piezoelectric transducers is nearly unanimous due to their ability to measure a large bandwidth of frequencies. Most waves generated from part degradation will occur between 50 kHz and 1 MHz [16].

Both passive and active AE methods use a similar approach for source location. Tobias discussed using these AE signals with an approach known as trilateration to estimate the location of the AE [17]. Tobias used a Hsu-Nielsen source, or a pencil lead break (PLB) to act as a repeatable AE source. This type of source utilizes a mechanical pencil to break an extended piece of lead to create an impulse on a test specimen. The test method is well described by Hsu [18] and Grosse [19]. Bozcar was able to statistically prove that pencil lead breaks are repeatable sources and of great use for AE testing [20]. This process was quickly adopted as a method of evaluating the functionality of an AE sensor array and has been utilized in experiments for many materials [21, 22, 23, 24].

Commercially available metal and semiconductor piezoresistive strain gauges are utilized for measuring static strain within a test specimen, while piezoelectric ultrasonic transducers are used for dynamic measurements. The USM sensor is a piezoresistive sensor that can capture both domains of information. The USM sensor has a wide frequency bandwidth and low minimum detectable strain, which allows for the simultaneous acquisition of quasi-static strain and acoustic emission information [21]. This capability has led to the study of measuring strain history and acoustic emissions from a single sensor to locate the crack tip during fracture for *in-situ* practices for NDE.

2. Materials and Methods

2.1 Governing Physics

2.1.1 Wave Propagation in Isotropic Plates

Wave propagation in plate-like structures has been well developed and outlined. By defining a plate as a load-carrying element that is substantially thin when compared to the length or width of the plate a special set of physics can be applied to the structure [22]. During excitation, two dominant wave modes are developed in a plate; a high frequency, high speed, lower energy symmetrical wave (also referred to as in plane or extensional waves), and a lower frequency, lower speed, higher energy antisymmetric wave (also referred to as out of plane or flexural waves). These waves are dispersive in isotropic materials such that their speed is dependent on the frequency of the wave. The formulation to develop dispersion curves are dependent on generic material properties such as the transverse and longitudinal wave velocities of a material which are consequently related to more obtainable material properties such as density, Young's modulus, and Poison's ratio. The development of the curve is given below [23].

$$c_T = \sqrt{\frac{E}{\rho}} \ and \ c_L = \sqrt{\frac{G}{\rho}} \tag{1}$$

Where the shear modulus, G, is equivalent to

$$G = \frac{E}{2(1 + \nu)} \tag{2}$$

The Rayleigh-Lamb Equations for plate waves are:

For symmetric waves:

$$\frac{tan(qh)}{q} + \frac{4k^2pqtan(ph)}{(q^2-k^2)^2} = 0 \tag{3}$$

Or antisymmetric waves

$$qtan(qh) + \frac{(q^2-k^2)^2tan(ph)}{4k^2p} = 0 \tag{4}$$

where k is the wave number, p is the wave number for the symmetric wave and p is the wave number for the antisymmetric wave.

$$k = \frac{\omega}{c_p} \tag{5}$$

$$p^2 = \left(\frac{\omega}{c_L}\right)^2 - k^2 \tag{6}$$

$$q^2 = \left(\frac{\omega}{c_T}\right)^2 - k^2 \tag{7}$$

By solving the roots of the Rayleigh-Lamb equations using Newton-Raphson's method, the phase velocity, c_p, can be found for a given wave frequency. By iterating through wave frequencies, the dispersion curves can be developed as seen below in figure 1. There may be multiple roots at a given frequency which indicates that there are multiple wave modes present at that frequency. This phenomenon is found at much higher frequencies than are found in the acoustic emission testing described in this report, hence the presented dispersion curves will only show the principal modes (A_0 and S_0). These are the dispersion curves for the lowest set of possible frequencies.

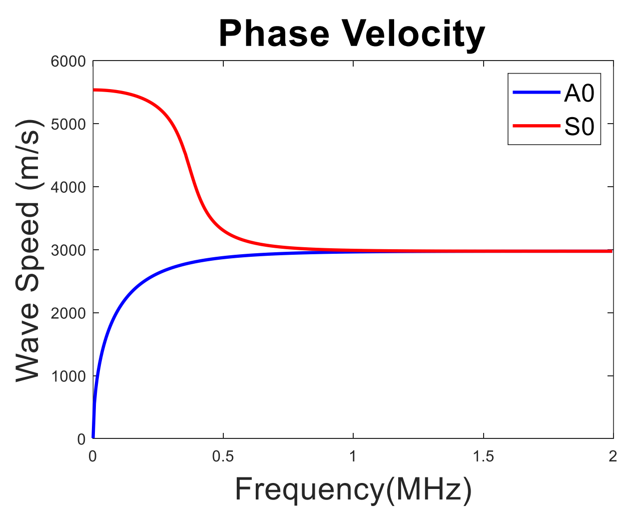

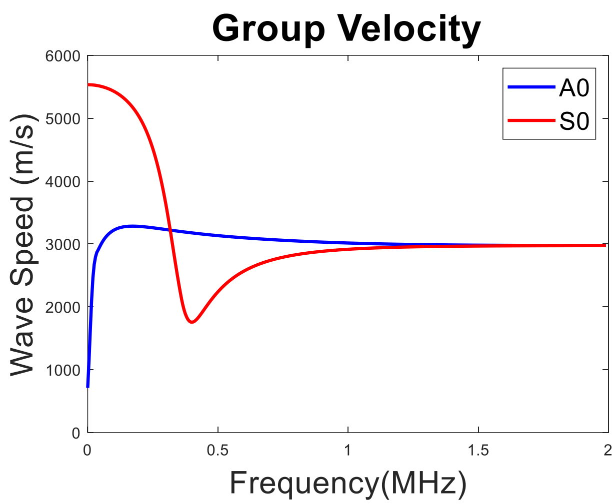

Figure 1: Phase and Group Velocity Curves of 6mm Aluminum Plate

It is critical to distinguish the difference between the phase and group velocities. The phase velocity is the rate at which a singular period of a wave mode is traveling. The group velocity is the rate which the entire wave mode, symmetric or antisymmetric is traveling. The initial wave arrival times are calculated from the first rising edge in the signal from the acoustic sensors such that the phase velocities are used.

2.1.2 Quasi-Static Fracture

In this study, the last experiment consists of loading a Compact Tension (CT) specimen in tension till failure due to fracture. The specimen was subjected to a quasi-static load such that the inertial effects can be ignored during the displacement of the specimen.

The crack length within a CT specimen can be estimated numerically from the applied load and stress intensity factor. The stress intensity factor, K, can be defined as [25],

$$K = \left(\frac{(2+\alpha)}{(1-\alpha)^{3/2}}(0.886 + 4.64\alpha - 13.32\alpha^2 + 14.72\alpha^3 - 5.64\alpha^4)\right)\cdot\left(\frac{P}{t\sqrt{b}}\right) \quad (8)$$

Once this is calculated for a given crack length, it must be compared to the critical stress intensity factor, K_{IC}, which is a material property. If the calculated stress intensity factor is greater than the critical stress intensity factor, fracture occurs.

It is important to note that K_{IC} is highly dependent on the thickness of the specimen [26]. The material properties and defining equations discussed in this paper are based around linearly elastic, plane strain specimens. To meet requirements for our experimental setup and still use standard equipment, the thickness had to be relatively thin such that plane-stress behavior is present [25].

2.1.3 Source Localization

Source localization refers to methods used for using various sensing technologies to estimate the location of a point of interest. Trilateration is a method of using three sensors to gather information to predict the location of a given source. This method was first developed for aerospace avionics in World War Two, and further modified for use with NDE. By creating a system of equations of three circles an intersection between all three can be determined to estimate the source of an acoustic emission [17].

$$\begin{cases} (x-h_1)^2 + (y-k_1)^2 = (r)^2 \\ (x-h_2)^2 + (y-k_2)^2 = (r+\delta_1)^2 \\ (x-h_3)^2 + (y-k_3)^2 = (r+\delta_2)^2 \end{cases} \quad (9)$$

Several inputs are required for successful source location. First, the cartesian coordinates for each sensor must be noted. These locations become the center of each circle in the system. Next, the difference in arrival times of the waves at each sensor must be calculated. This is a simple calculation such that,

$$\Delta t = t_1 - t_2 \quad (10)$$

$$\delta = \Delta t * v \quad (11)$$

Once a difference in arrival time, Δt , has been calculated, a difference in distance, δ, can then be calculated. This is done by accounting for the wave speed. This can be done by utilizing the dispersion curves and interpolating for a wave velocity or by using a constant value based on the material properties. For this study, a wave speed of the antisymmetric wave of 3100 m/s was used to use to simplify source location calculations. This information can now be input into the following equations [17].

$$A_1 = x_1^2 + y_1^2 - {\delta_1}^2 \quad (11)$$

$$A_2 = x_2^2 + y_2^2 - {\delta_2}^2 \quad (12)$$

$$B = \sqrt{(A_1x_2 - A_2x_1)^2 + (A_1y_2 - A_2y_1)^2} \quad (13)$$

$$K = \frac{A_2\delta_1 - A_1\delta_2}{B} \quad (14)$$

$$\varphi = \tan^{-1}\left(\frac{A_1y_2 - A_2y_1}{A_1x_2 - A_2x_1}\right) \quad (15)$$

$$\theta = \arccos(K) + \varphi, r > 0 \quad (16)$$

$$\theta = \arccos(\mathrm{K}) + \varphi + \pi,\ r > 0 \quad (17)$$

$$r = \frac{A_1}{2\left(x_1\cos(\theta) + y_1\sin(\theta) + \delta_1\right)} \quad (18)$$

This evaluation gives the circular coordinates of the estimated AE source location and can easily be converted to x-y coordinates.

Due to rounding differences during the time of the wave arrival, the three circles overlap within a few millimeters of each other and do not perfectly intersect. In this case the location for which the three circles intersect most closely were selected and the x-y coordinates of the intersection were averaged together to determine a singular point for the estimated location source.

2.2 Materials

2.2.1 Commercial Sensors Used

An Omega linear metal strain gauge was used for comparison in strain measurement to the USM Sensor. The strain gauge has a gauge factor of 2.07, a resistance of 350 ohm and a tolerance of .2%.

Three Briktek Ultrasonic Transducers were used during testing for comparison to the USM Sensor during AE source monitoring. The transducers utilize a lead zircon titanate (PZT) sensing element and have a natural frequency of 2.25 MHz.

An Instron 3369 Load Frame was used for the tensile testing conducted in this study. The load frame had a 50 kN load cell with an accuracy of 0.5%. The provided Bluefield software was used for test control and acquisition of load cell measurements.

2.2.2 Physical Materials

All test specimens in this report were constructed of 6061-T6 aluminum. The relevant material properties are shown below [27]

Density (kg/ m3)	Young's Modulus (Gpa)	Poison's Ratio	K_{IC} (MPa-m½)
2700	69	.3	29

Table 1: 6061-T6 Material Properties

For the Pencil Lead Break (PLB) tests discussed in this report, 3 diameters of lead were used. Pentel 2H .7mm and .5mm leads were used in addition to 3H .3mm lead. 2H and 3H refer to the relative stiffness of the lead.

2.2.3 Data Collection and Instrumentation

For all testing a PicoScope 4824 8 Channel Oscilloscope and Data Acquisition unit was used. The PicoScope was grounded to an external power supply and the test sample.

Several conditioning units were used throughout testing to filter and amplify the sensor signal for both the commercial and USM sensors.

For tests with the USM sensor an external signal conditioning unit (SCU) was used. This three-channel device contains a Wheatstone bridge to generate a signal voltage from the resistance change the USM sensor. A Texas Instruments INA849 High-Speed Amplifier was used for signal amplification. A Texas Instruments THS 4022 Dual Op Amp was used for a 700 kHz lowpass filter to remove unwanted noise from voltage switching. This SCU is further discussed in Appendix B.

For the quasi-static fracture study, the ultrasonic transducers were amplified by 10 dB and filtered using a high-pass RC filter consisting of a 1 microfarad capacitor and a 680 ohm resistor, resulting in a high-pass frequency of 5 kHz. This was used to remove low-frequency noise from the Instron load frame during testing.

2.3 Experimental Setup

2.3.1 Test 1: Static Pencil Lead Break Test

A pencil lead break (PLB) test was performed at 5 different locations on an aluminum plate to analyze the effectiveness of the USM sensor for source location.

A 6061-T6 plate that was 350mm x 350mm with a thickness of 2.2mm was used. An array was constructed on the plate with permanent marker of 25x25mm squares to promote repeatable location of the pencil lead break tests. A representation of the test plate along with the physical test plate with sensors are shown below.

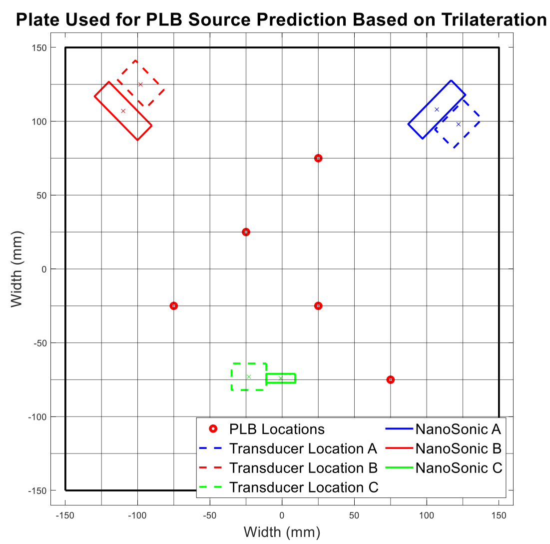

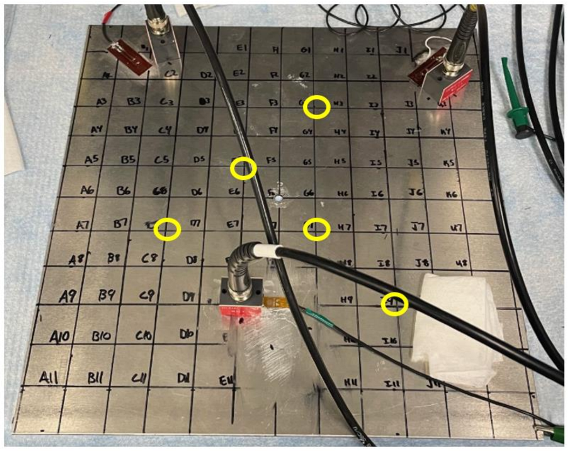

Figure 2: Physical test plate and along with blank test plate used for visualization

The columns of the array are labeled alphabetically from left to right, while the rows are numbered from top to bottom. Five locations were selected for this study, their name and coordinates are

Location Name	Coordinates
C7	(-75,-25)
E5	(-25,25)
G3	(25,75)
G7	(25,-25)
I9	(75,-75)

Table 2: Locations of PLB test locations

For each of the three lead thicknesses, PLB tests were performed at each of the five locations. At each location, the test was repeated 5 times.

2.3.2 Test 2: Pencil Lead Break Test Under Tension

A second pencil lead break test was conducted, and included strain measurement by subjecting the previously mentioned 350x350mm 6061-T6 Aluminum plate to a tensile load. It was proven the USM sensors can provide comparable results to the commercial ultrasonic transducers, this test was the first test to prove the dual-use capabilities of the USM sensor.

Much of the experimental procedure was the same as described for Test 1. A notable change is that the plate is no longer resting flat on a tabletop and is instead held by the two Instron jaws at the top and bottom of the plate.

Figure 3: Test setup for tensile PLB test

The plate was loaded at .1mm/min to remove any inertial effects due to loading, and to allow for ample time to conduct the pencil lead break tests before over-ranging the signal of the USM sensor, see Appendix B for more information. The same five test locations were used as in Test 1 and the .3mm PLB was repeated five times at each location.

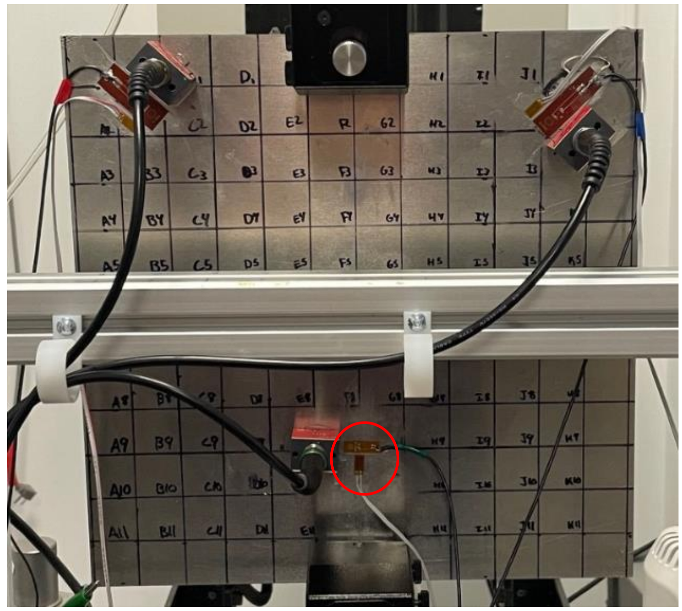

Figure 4: Sensor location for tensile PLB test

During the test. two different time domains were recorded for separate strain and acoustic emission measurements. A long-term time domain was used to measure the strain behavior on the plate. The USM and metal strain in the circled region of the plate were observed so the sensors were located on the axis of the applied load. This was done since the two other sensor pairs in the top corners were in regions of low strain as shown in the strain plot in figure 5.

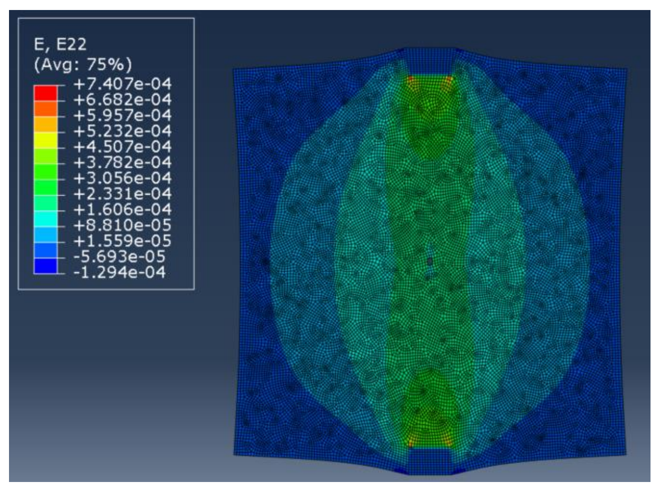

Figure 5: Strain plot of test specimen for tensile PLB test

For the strain measurement was recorded for the entire duration of the test at 200 Hz, while capturing the DC shift of a commercial strain gauge and USM sensor. This DC shift can consequently be used to find the strain at the mounting location with the use of the gauge factor of the sensor.

The second time domain used was a short-term window used to measure the acoustic emissions of the PLBs for source location. Information from the USM sensors and ultrasonic transducers was recorded in 50ms windows at 2 MHz.

2.3.3 Test 3: Quasi-Static Fracture Monitoring

This study sought to compare the USM sensor to commercial sensors in two measurement categories, strain and acoustic emissions. The difference between the two studies is that fracture monitoring will demonstrate the USM sensor in a situation that would be a useful field application of this technology.

For this test, a compact tension (CT) specimen was used due to its application in fracture and crack growth studies. The specimen's outer dimensions were 150x150mm and was constructed of 6mm thick 6061-T6 aluminum. Further considerations and discussion of the test specimen can be found in Appendix A.

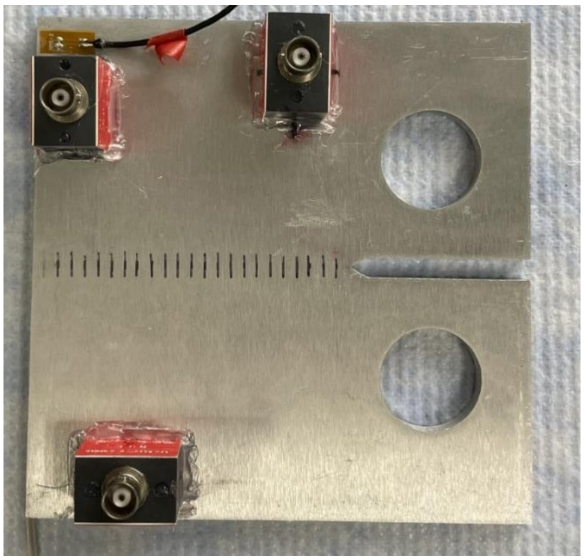

Figure 6: CT specimen with sensors for crack propagation test

For the acoustic emission measurements conducted in this test, 3 commercial ultrasonic transducers and 1 USM sensor were used. The four sensors were then considered as two separate groups for source location estimation, one group consisted entirely of the transducers while the other consisted of two transducers and the sensor. This was done to show the change in location accuracy when utilizing the sensor. The data for this test was gathered in a similar manner to the previous tests, using a 50ms window captured at 20 MHz.

A commercial strain gauge and USM sensor were used for comparison of strain measurement during this test. The sensors were placed symmetrically on the opposite sides of the test specimen to capture identical strain for accurate data comparison. This information was gathered during the entire duration of the test at 200 Hz.

The signal conditioning of these sensors was modified for this test. The commercial transducers were amplified and filtered with a high pass filter. Amplification was required to detect the low energy emissions from crack propagation. The high pass filter was used to remove any extraneous noise from the testing environment and the Instron machine itself. The USM sensor used an alternate signal conditioning board that physically decouples the AC and DC components of the sensor signal using a high pass filter. Both boards are further elaborated upon in Appendix B.

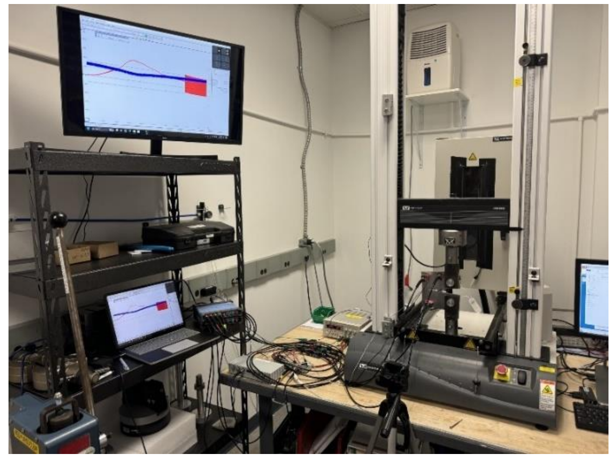

Figure 7: Test setup for crack propagation test

For this test, the CT specimen was loaded at 2mm/min for 8 minutes reaching a maximum vertical displacement of 16mm. This load rate was selected to slowly load the plate to remove any inertial effects.

3. Results and Discussion

3.1 Pencil Lead Break Tests

The diameter of the pencil lead significantly impacted the peak amplitude of the measured acoustic emission. A higher energy emission being represented by the .7mm lead and a lower energy acoustic emission being represented by the .3mm lead. The respective energy levels are shown below

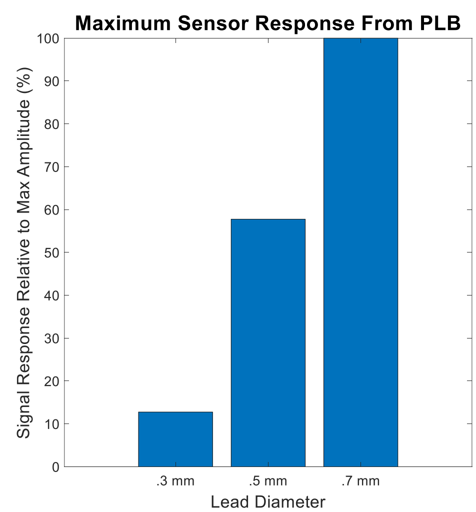

Figure 8: Comparison of AE amplitude from different lead thicknesses

The recorded emissions amongst all PLB tests showed consistency in their responses. Figure 9 highlights an example response of both a USM sensor and a commercial ultrasonic transducer. The transducer signal is the raw output, while the USM signal has been filtered with a 5 kHz high pass filter to remove low frequency noise and DC shift.

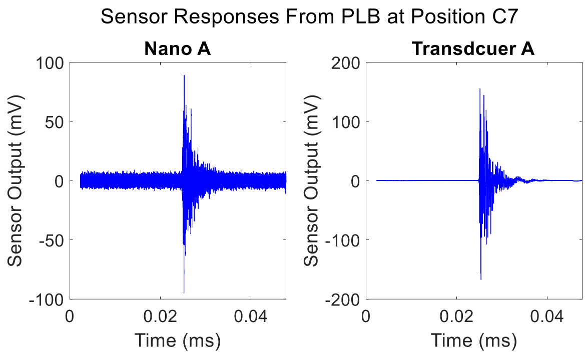

Figure 9: Example of sensor signals from PLB

The signal to noise ratio (SNR) of the USM sensor is noticeably less than the commercial ultrasonic transducer. For both sensors, the SNR increases with lead diameter. These values are tabulated below.

	USM (dB)	Transducer (dB)
.3 mm	14.8	42.4
.5 mm	25.4	52.8
.7 mm	31.9	59.3

Table 3: Signal to noise ratios from PLB

The time-of-flight differences for the 5 repeated tests at each PLB location were averaged together for use with trilateration. The individual time of flights was used to generate a 95% confidence interval. In the figures below the dotted circles represent the upper bound of this confidence interval.

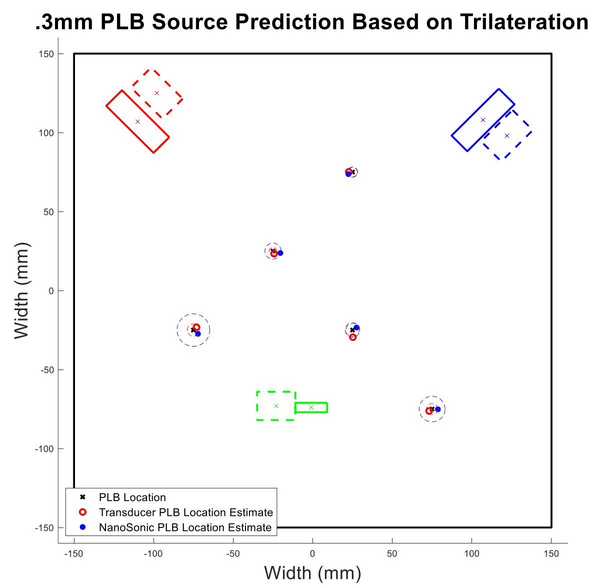

Figure 10: .3mm PLB source location results

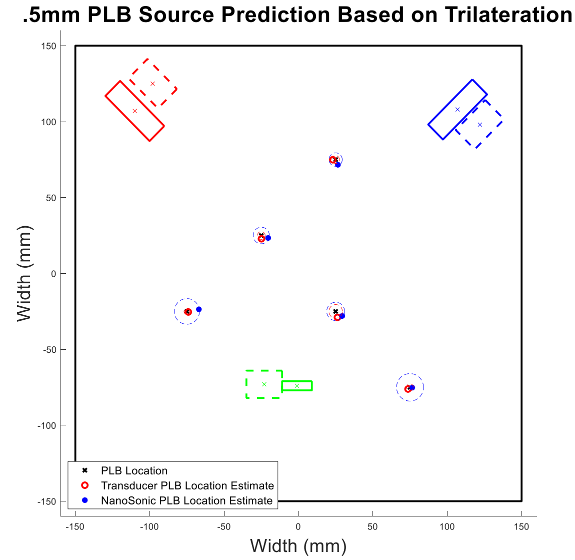

Figure 11: .5mm PLB source location results

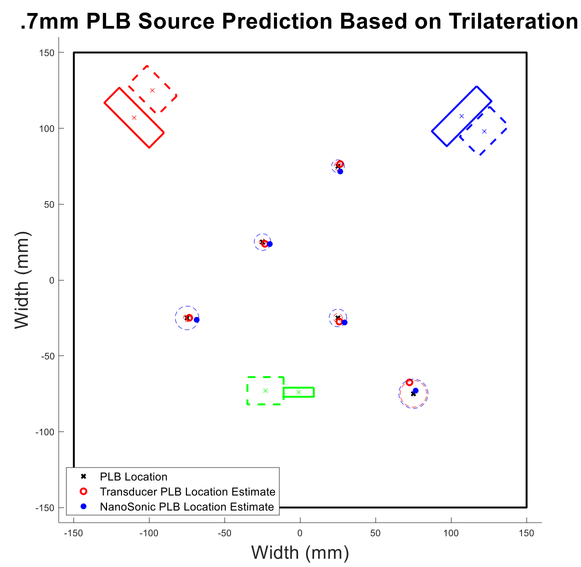

Figure 12: .7mm PLB source location results

The commercial ultrasonic transducers and USM sensors were able to achieve source location estimates within 10mm of the actual location. The distance the source location estimates were from the actual PLB location are given in the table below.

	.3mm		.5mm		.7mm	
Location	Transducer	USM	Transducer	USM	Transducer	USM
C7	2.76	4.79	1.03	8.16	1.48	6.50
E5	2.65	3.72	2.16	4.88	1.97	5.00
G3	2.40	2.89	1.93	3.73	2.08	3.73
G7	4.50	2.99	4.11	5.33	2.59	5.33
I9	2.25	3.63	1.76	1.53	7.95	2.53

Table 4: Distance between AE source and estimated location (in mm)

The accuracy did not appear to correlate to the lead diameter, despite the wave arrivals being of greater amplitude. For the .3mm testing, the test with the worst signal to noise ratio, the initial wave arrivals were greater in amplitude than the noise floor. The cause of inaccuracies could be caused by the location of the PLB test. A preexisting hole at the center of the plate could distort the surface wave or reflect the wave such that the arrival time is delayed. In this test, a shift in arrival time of 1 microsecond could modify the location estimate by over 5mm.

3.2 Tensile PLB Test

The result of the trilateration estimates for the sources of the .3mm PLB under tension using the average time of flight for the five tests are shown below.

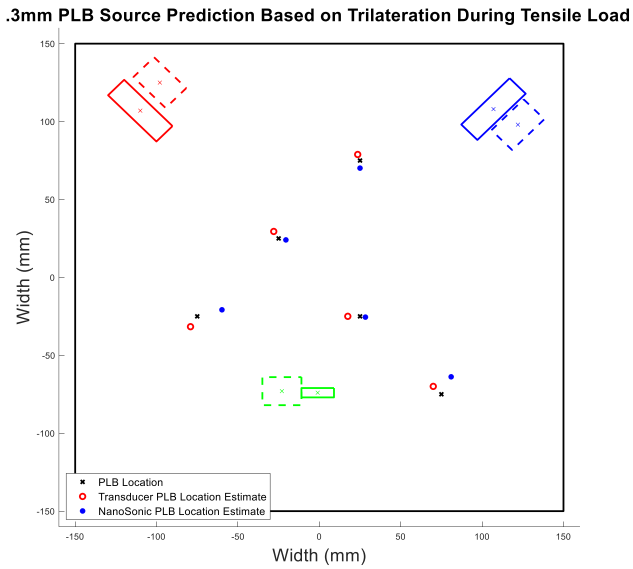

Figure 13: .3mm Trilateration Estimates for Tensile PLB Test

The results of these source location estimates are similar to Test 1, with the center most points having the highest accuracy and the outer points having less accuracy. The USM sensors are penalized more when estimating outside the sensor array, having a greater decrease in accuracy than the commercial transducers. However, inside the sensor array the USM sensors have equivalent or sometimes superior accuracy. These results are tabulized below.

	.3mm Dynamic	
Location	Transducer	USM
C7	7.83	15.74
E5	5.40	4.56
G3	4.13	4.88
G7	7.51	3.35
I9	7.11	12.70

Table 5: Distance between AE source and estimated location (in mm)

For the strain measurement, three sets of data will be compared. The USM sensor and the commercial strain gauge were placed next to each other on the loaded axis of the plate to read similar strain values. The values from the Instron load cell will also be used for comparison. Due to the linearly elastic nature of this test, the slopes of all three datasets when comparing strain or load versus time should be nearly identical. The three datasets are plotted on the same graph, with each set of data normalized such that the maximum value is 100% for ease of comparison.

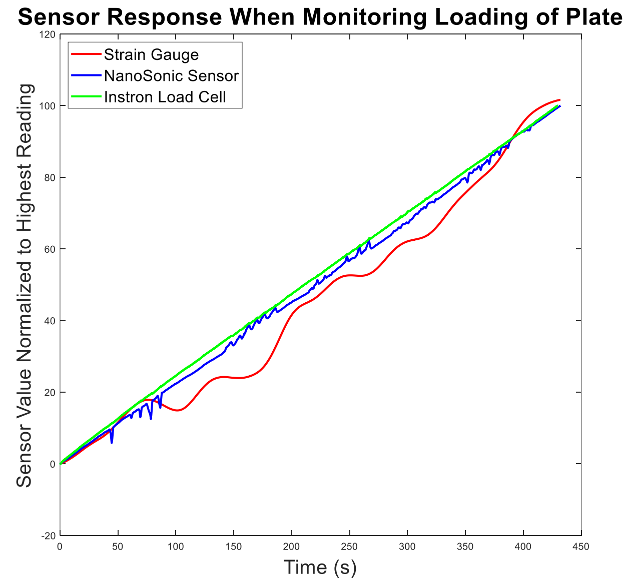

Figure 14: Sensor Response to Loading of Plate

The results from the strain and acoustic emission measurements illustrate the USM sensor's ability to simultaneously measure this information. The USM sensor was able to estimate acoustic emission locations within several millimeters of the commercial sensor. Additionally, the USM sensor was able to measure the strain with great relativity to both the commercial strain gauge and the load cell of the Instron machine. This information gives confidence in the USM sensors applicability for fracture monitoring where both pieces of information are critical.

3.3 Quasi-Static Fracture Monitoring

During the quasi-static fracture test, eleven emissions were recorded from the CT specimen. The amplitude of the emissions varied from values similar to the previous PLB tests to just 50% of even the lowest SNR. Even at these SNRs, the USM sensor was still able to perform well. The minimum SNRs are given in the table below.

	USM (dB)	Transducer (dB)
Min SNR	7.7	29.9

Table 6: Minimum SNR during crack propagation

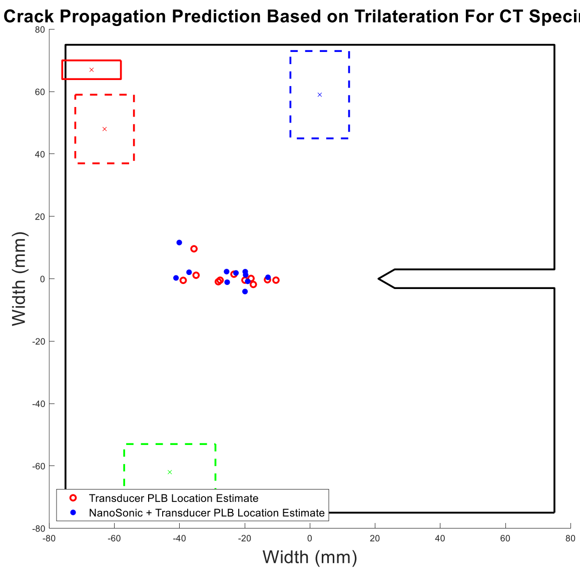

Figure 15: Crack propagation prediction from both sensor arrays

The estimations of the crack tip location based of the sensor information are shown in the figure above. The results demonstrate that the USM and the commercial sensor arrays can predict the crack tip location at the middle and end of its path.

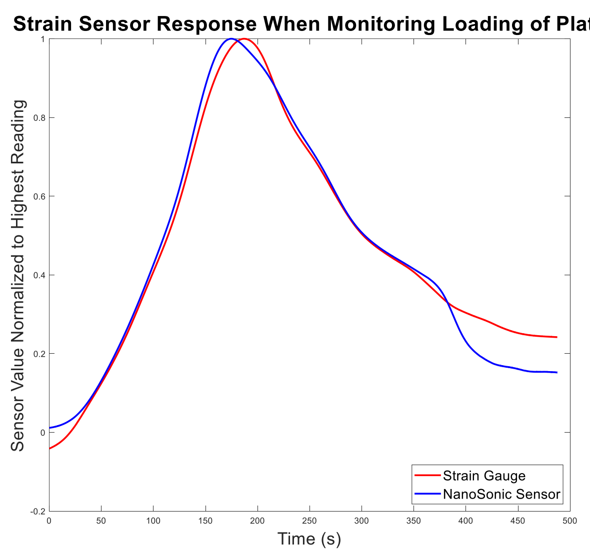

Figure 16: Strain sensor readings on CT specimen

The strain information from the USM sensor and strain gauge both follow nearly identical trends with a deviation only occurring at the end of testing as shown above. This error was due to a malfunction with the signal conditioning unit inducing excess noise into the raw signal. Both signals were filtered with a gaussian filter to smooth any high frequency noise.

4. Conclusion and Future Work

The NanoSonic USM sensor highlights the foundational principles of acoustic emission testing for NDE pioneered by Kaiser and Dunegan by successfully monitoring the strain and emitted AEs to quantify the degradation of a component. The USM sensor has been demonstrated to successfully monitor AEs in both static and dynamic loading scenarios of thin plates. On a specimen subjected to a load, the USM sensor was shown to be able to monitor the strain history of the structure with similar results to a commercial metal strain gauge. This was then applied to a quasi-static fracture study where the USM sensor was able to detect low energy emissions from ductile fracture for source location methods. Additionally, during fracture, the USM sensor was able to accurately monitor the elastic-plastic strain during the failure of component. This makes the USM sensor the first piezoresistive sensor capable of simultaneously measuring both high and low frequency events. This consolidation of data acquisition can provide large advancements to the fields of SHM and NDE by providing a multimodal, small form factor sensor that can be used in a multitude of applications.

The presented work increased the practicality for field use of the NanoSonic USM sensor. Crack growth is a widely investigated topic and can cause catastrophic damage if not monitored properly. Quasi-static loading for crack growth is the first step of this investigation. Further studies can include fatigue crack growth in metallics, and delamination of composites. The CT specimen was used for its transferability and applicability to fatigue studies, although a fatigue resistant alloy such as 7075-T6 should be substituted as shown in the study presented by Keshtegar [15]. The USM sensor can provide a unique opportunity for delamination studies due to its compact design. The thin silicon membrane could allow for inter-layer, embedded sensing like discussed by Janeliukstis [28]. To develop a system that can be used for *in-situ* use, a system that can automatically determine the arrival times of the surface waves should be further investigated. Manual parsing is the most reliable method, but time consuming for large data sets and requires an experienced user. Several approaches have been investigated and discussed in literature. The simplest discussed by Gorman utilizes cross correlation but would require the signals from each sensor to be nearly identical. A more universal, though more computationally heavy would be the statistical approaches discussed by Allen, and further built upon by Takanami and Dong [29, 30, 31]. Automation of this process would allow for location of AE events and component health monitoring without user input. This sort of autonomy would add to the in-situ use of the USM sensor cementing its place in NDE.

Acknowledgement

The material and subsequent research conducted in conjunction with this paper was supported in part by NASA under contract 80NSSC22CA085. We would like to thank William C. Wilson for his support and insight during the project.

References

[1] W. K. Farrar R. Charles, "An introduction to structural health monitoring," *Philosophical Transactions of the Royal Society A,* vol. 365, no. 1851, 2007.

[2] M. Trimm, " An overview of nondestructive evaluation methods," *Practical Failure Analysis ,* vol. 3, pp. 17-31, 2003.

[3] L. D. A. V. Z. D. V. G. Gabor Por, "Acoustic Emission during tensile tests and ECAP," in *30th European Conference on Acoustic Emission Testing & 7th International Conference on Acoustic Emission*, Granada, 2012.

[4] R. B. D. H. L. Engle, "ACOUSTIC EMISSION: STRESS WAVE DETECTION AS A TOOL FOR NONDESTRUCTIVE TESTING AND MATERIAL EVALUATION," *8th Symposium on Physics and Nondestructive Testing,,* 1968.

[5] M. O. Christian U. Grosse, Acoustic Emission Testing: Basics for Research - Applications in Civil Engineering, Berlin: Springer-Verlag, 2008.

[6] T. M. J. E. M. Bao Mi, "In-situ ultrasonic monitoring of crack growth under static and dynamic loading conditions," in *The International Society for Optical Engineering*, 2005.

[7] S. H. T. S. T. Arakawa, "The detection of weld cracks using ultrasonic testing," *NDT International,* vol. 18, no. 1, pp. 9-16, 1985.

[8] S.-T. L. Shiuh-Chuan Her, "Non-Destructive Evaluation of Depth of Surface Cracks Using Ultrasonic Frequency Analysis," *Ultrasonic Sensors and Transducers for Applications in Biology, Medicine and NDT,* 2014.

[9] P. G. T. T. T. S. J. C. D. S. R. a. D. J. D. Heasler, "Ultrasonic inspection reliability for intergranular stress corrosion cracks," USNRC, 1990.

[10] R. H. J. B. T.M. Morton, "Acoustic emissions of fatigue crack growth," *Engineering Fracture Mechanics,* vol. 5, no. 3, pp. 693-697, 1973.

[11] M. T. T.M. Roberts, "Acoustic emission monitoring of fatigue crack propagation," *Journal of Constructional Steel Research,* vol. 59, no. 6, pp. 695-712, 2003.

[12] P. G. U. &. K. A. Vanniamparambil, "Identification of Crack Initiation in Aluminum Alloys using Acoustic Emission," *Experimental Mechanics,* vol. 55, pp. 837-850, 2015.

[13] S. M. V. G. V. G. P. Z. J. Y. Lingyu Yu, "Dual Mode Sensing with Low-Profile Piezoelectric Thin Wafer Sensors for Steel Bridge Crack Detection and Diagnosis," *Advances in Civil Engineering,* vol. 2012, pp. 1-10, 2011.

[14] E. B. M. D. R. E. M. A. Dris, "A0 Lamb Mode Tracking to Monitor Crack Evolution in Thin Aluminum Plates Using Acoustic Emission Sensors," *Applied Sciences,* 2022.

[15] C. M. S. M. M. Azadeh Keshtgar, "Structural Reliability Prediction Using Acoustic Emission-Based Modeling of Fatigue Crack Growth," *Applied Sciences ,* vol. 8, 2018.

[16] N. J. E. M. N. N.Morizet, "Classification of acoustic emission signals using wavelets and Random Forests : Application to localized corrosion," *Mechanical Systems and Signal Processing,* vol. 70, pp. 1026-1037, 2016.

[17] A. Tobias, "Acoustic-emission source location in two dimensions by an array of three sensors," *Non-Destructive Testing,* vol. 9, no. 1, pp. 9-12, 1976.

[18] B. F. Hsu N., "CHARACTERIZATION AND CALIBRATION OF ACOUSTIC EMISSION SENSORS," *Material Evaluation,* vol. 39, pp. 60-68, 1981.

[19] C. Grosse, "NDT.net," 07 09 2002. [Online]. Available: https://www.ndt.net. [Accessed 26 06 2024].

[20] T. B. a. M. Lorenc, "The repeatability and reproducibility of calibrating signals," *Journal de Physique IV,* 2005.

[21] Y. K. A. d. C. S. M. N. J. J. D. A. W. H. R. W. N. J. Stiefvater, "Dual-Use Strain Sensors for Acoustic Emission and Quasi-Static Bending Measurements," *Sensors,* vol. 24, no. 5, 2024.

[22] P. G. Lowe, Basic Principles of Plate Theory, 1982 .

[23] J. L. Rose, Ultrasonic Guided Waves in Solid Media, Cambridge University Press, 2014.

[24] R. D. Sridhar Santhanam, "Reflection of Lamb waves obliquely incident on the free edge of a plate," *Ultrasonics,* vol. 53, no. 1, pp. 271-282, 2013.

[25] S. L. K. M. V. K. Norman E. Dowling, Mechanical Behavior, Pearson Education , 2020.

[26] W. F. M.O. Lai, "Effect of specimen thickness on fracture toughness," *Engineering Fracture Mechanics,* vol. 23, no. 4, pp. 649-659, 1986.

[27] T. L. G. Howard E. Boyer, Metals Handbook, Vol.2 - Properties and Selection: Nonferrous Alloys and Special-Purpose Materials, 1990.

[28] D. M. R. Janeliukstis, "Smart Composite Structures with Embedded Sensors for Load and Damage Monitoring – A Review," *Mechanics of Composite Materials,* vol. 57, pp. 131-152, 2021.

[29] M. R. G. Steven M. Ziola, "Source location in thin plates using cross-correlation," *JASA,* vol. 90, no. 5, pp. 2551-2556, 1991.

[30] G. K. Tetsuo Takanami, "A new efficent procuedurefor the estimation of onset time for seismic waves," *Physical Earth,* vol. 36, pp. 267-290, 1988.

[31] S. B. Y. Z. Q. H. a. H. Z. L. Dong, "Arrival-Time Detection With Multiscale Wavelet Analysis and Source Location of Acoustic Emission in Rock," *Sensors,* vol. 23, no. 14, pp. 16313-16323, 2023.

[32] M. O. D. G. A. T. S. a. S. (. S. A. E. T. :. B. f. R. -. A. i. E. C. S. I. P. I. S. 2. 1. C. U. Grosse.

[33] S. C. P. K. Pierre Duchene, "Acousto-ultrasonic damage evaluation of carbon fibre composites using pencil lead break sources," in *18th European Conference on Composites Materials*, Athens, 2018.

[34] X. B. S. V. N. R. C. R. L. R. F. R. C. D. a. W. K. C. Yao, "Modal Decomposition of Acoustic Emissions from Pencil-Lead Breaks in an Isotropic Thin Plate," *Sensors,* vol. 23, 2023.

[35] V. S. R. A. J. M. C. P. Z. Ramin Madarshahian, "Hsu-Nielsen source acoustic emission data on a concrete block," *Data in Brief,* vol. 23, 2019.

[36] A. F. N. S. J. Prathuru, "Application of Pencil Lead Break (PLB) Point Source in the Detection of Interfacial Defects in Adhesive Bonds," *Journal of Nondestructive Evaluation,* vol. 41, 2022.

Appendix A: Determination Of CT Specimen

For the quasi-static fracture test several considerations were considered during the overall design of the experiment. The first was defining the overall geometry of the test specimen. A geometry that can be repeatable and well modeled by analytical solutions was desirable. The compact tension (CT) specimen was an ideal choice as a quantified testing procedure and solution for force vs crack length has been well defined. Further defining specimen geometry, it was found during preliminary testing and has been well documented in literature that increasing the distance between acoustic sensors for source location will often increase resolution. In conjunction with the size constraints of the Instron load frame, a maximum size of CT Specimen was defined as 150x150 mm. The in-plane dimensions of the specimen are shown below.

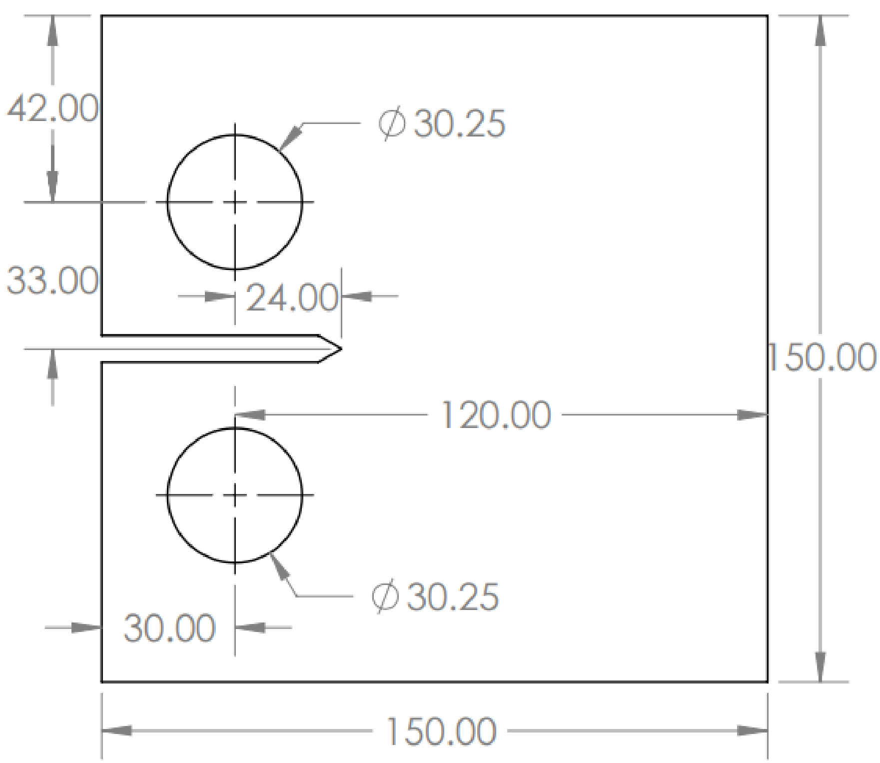

Figure A1: Dimensions of proposed CT specimen shown in millimeters (mm)

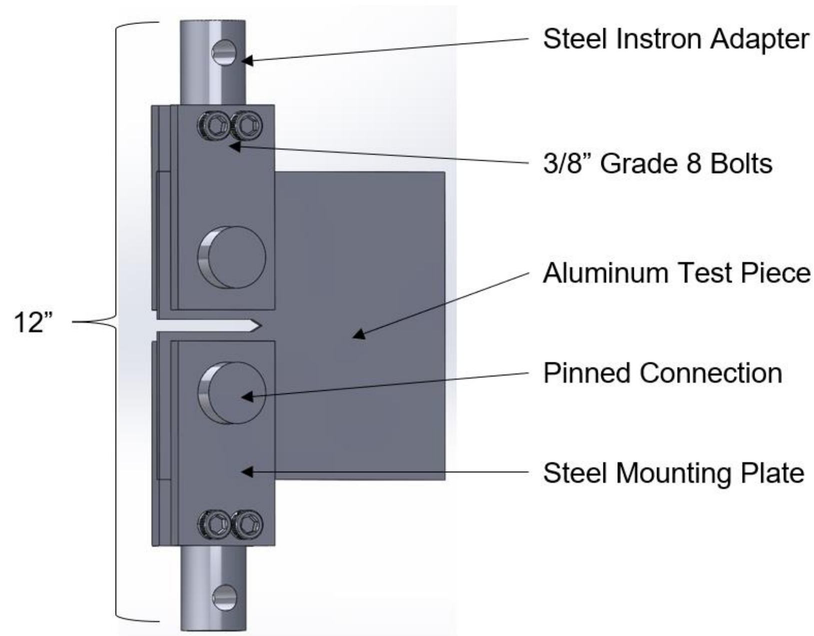

Figure A2: Test setup for CT specimen

An additional geometric consideration was the out-of-plane thickness of the specimen. Since most material properties defining fracture are defined for plane-strain situations, it was desired to maximize the thickness of the specimen. Plane-strain refers to a specimen that does not experience any strain in the thickness dimension, and only experiences strain in the in-plane axes. This phenomenon is seen in thick specimens. Due to limitations in the maximum load that can be applied by the load frame, thin 3mm and 6mm specimens were tested to evaluate the maximum force required for fracture. These thin specimens create plane-stress conditions causing there to be no stress through thickness of the specimen. The maximum load of the load frame (50kN) was achieved when testing with a 6mm 6061-T6 test specimen and was thus selected for further testing.

Another consideration was material selection. Wrought aluminum such as 2024-T4, 6061-T6, and 7075-T6 are very common in the Aerospace industry due to their high strength to weight ratios, ductility, and workability. 2024-T6 and 7075-T6 also have an improved fatigue resistance. All 3 wrought alloys will fail due to ductile fracture. MIC6 is a cast aluminum which is significantly more brittle than wrought aluminum and was used to aid in the comparison of results between ductile and brittle fracture. It was found that while nearly the same number of emissions were recorded for each specimen, ~ 40 emissions, the cast aluminum completely fractured in less than 5 seconds. The 6061-T6 specimen used was pulled at the same rate of 2mm/min for 8 minutes during which the specimens failed due to stable ductile fracture. The figures below show the difference between the two fracture types. The angled nature of the crack of the 6061-T6 specimens are an indication of ductile fracture. The 6061-T6 was selected for further testing due to the longer window for emission monitoring, and higher applicability to the Aerospace industry.

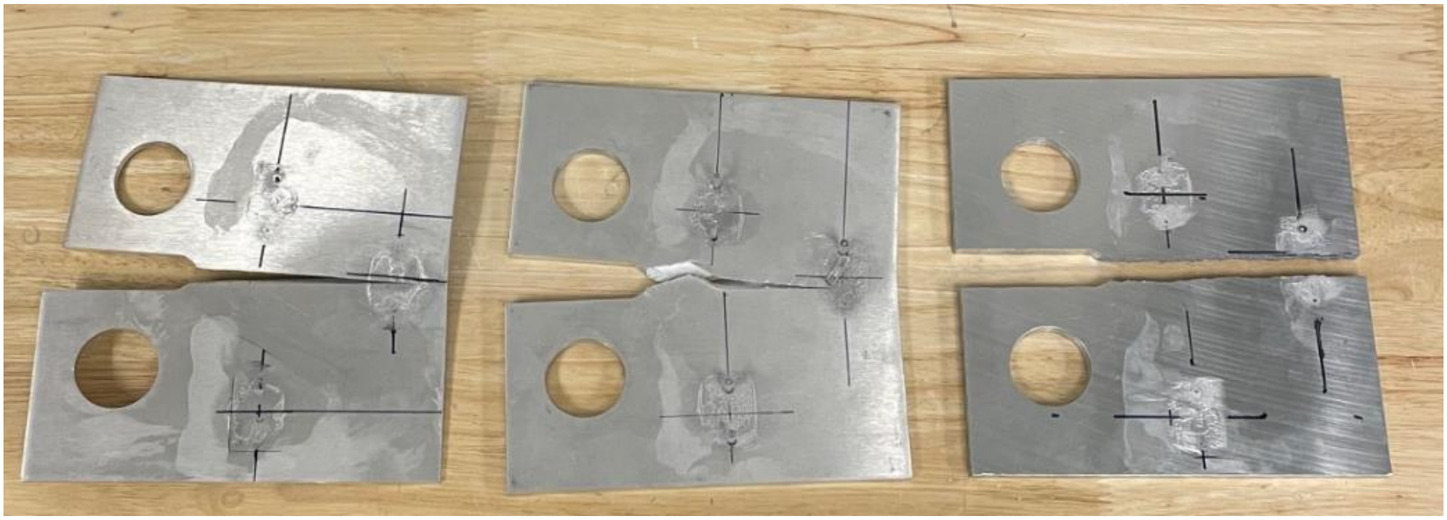

Figure A3: Comparison of different materials used for preliminary CT Specimen testing left to right: 1/8" 6061-T6, ¼" 6061-T6, ¼" MIC6

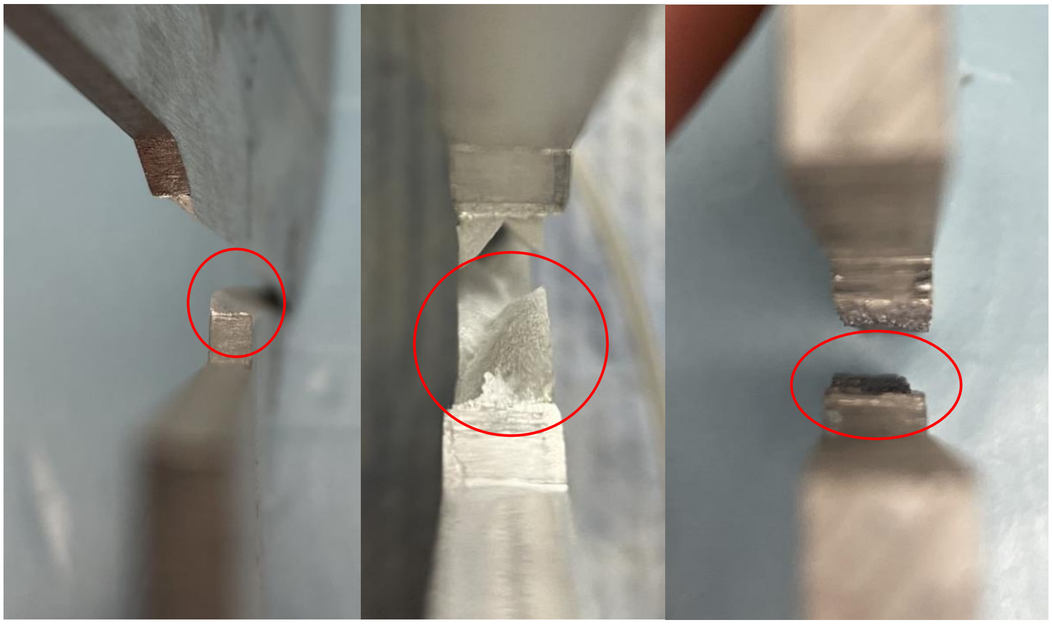

Figure A4: Images showing different crack profile of each specimen left to right: 1/8" 6061-T6, ¼" 6061-T6, ¼" MIC6

The final step of evaluating the test specimen was done by validating the placement of the NanoSonic USM sensor for testing. This was done with FEA simulations and comparing the results with data from experiments with commercial sensors. A virtual crack closure model (VCCT) was used to simulate the test in an ABAQUS explicit model. The model first assumed a linear elastic model with material properties defined below. Quadratic second-order plane stress elements (CPS8) were used for this model due to their ability to handle large deformations better than a first-order element.

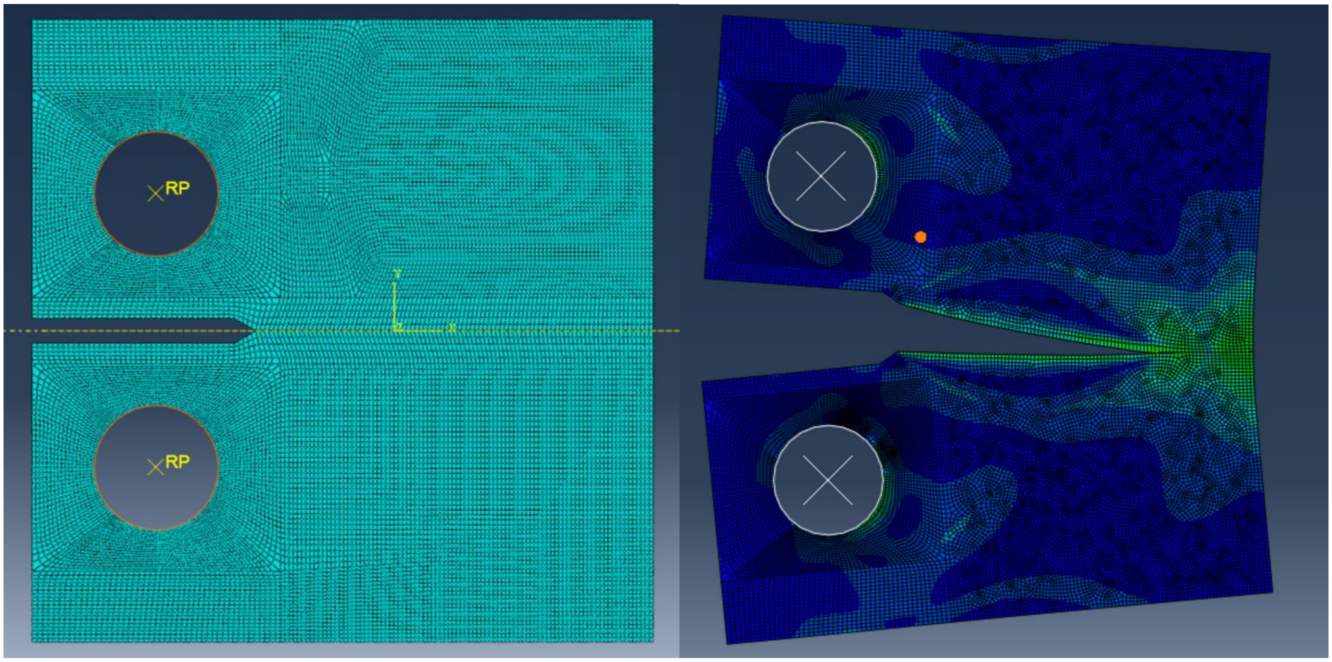

Figure A5: Mesh and deformed plastic-elastic model in ABAQUS

This yielded a result that suggested a maximum load that was much too low when compared to experimental data yet aligned with the analytical solution of the CT Specimen, as shown in figure A6. Plasticity was then added to the model which improved the result to more closely correlate with the experimental data.

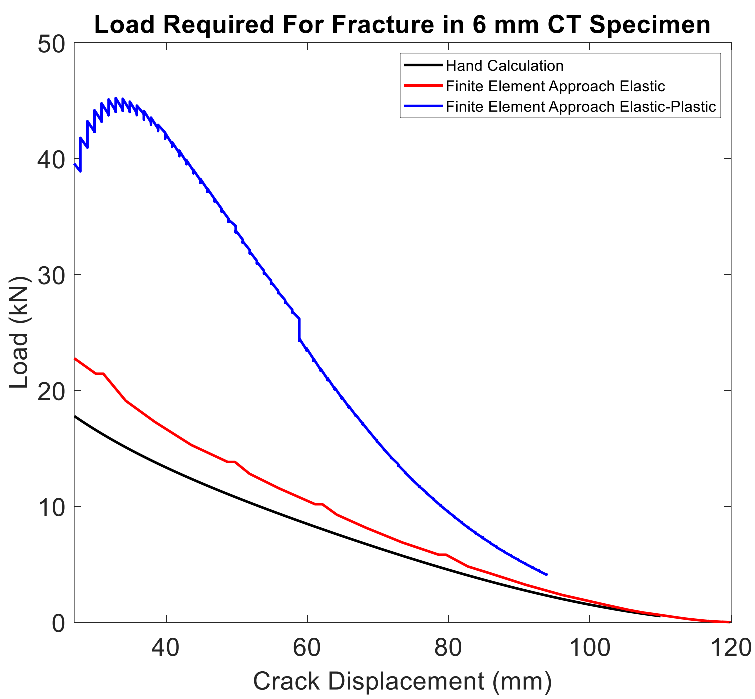

Figure A6: Comparison of crack length vs load in 6mm thick CT specimen for analytical solutions vs elastic and elastic-plastic finite element models

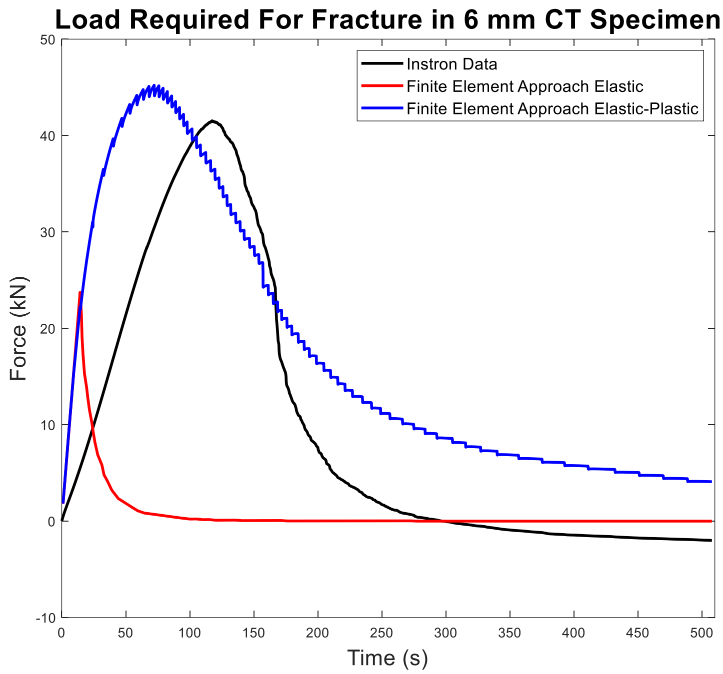

Figure A7: Time history of loading required for ductile fracture in 6mm thick CT specimen from load cell data vs elastic and elastic-plastic finite element models

Once the critical load correlated to the experimental data, the model was partitioned to include multiple areas of interest where strain gauge data had been gathered. The time history plots of these strain values are shown below. The USM sensor has been validated to a maximum strain value of 1000 microstrain. The goal of this study is to determine a location that satisfies this criterion for the placement of the USM sensor for the final test.

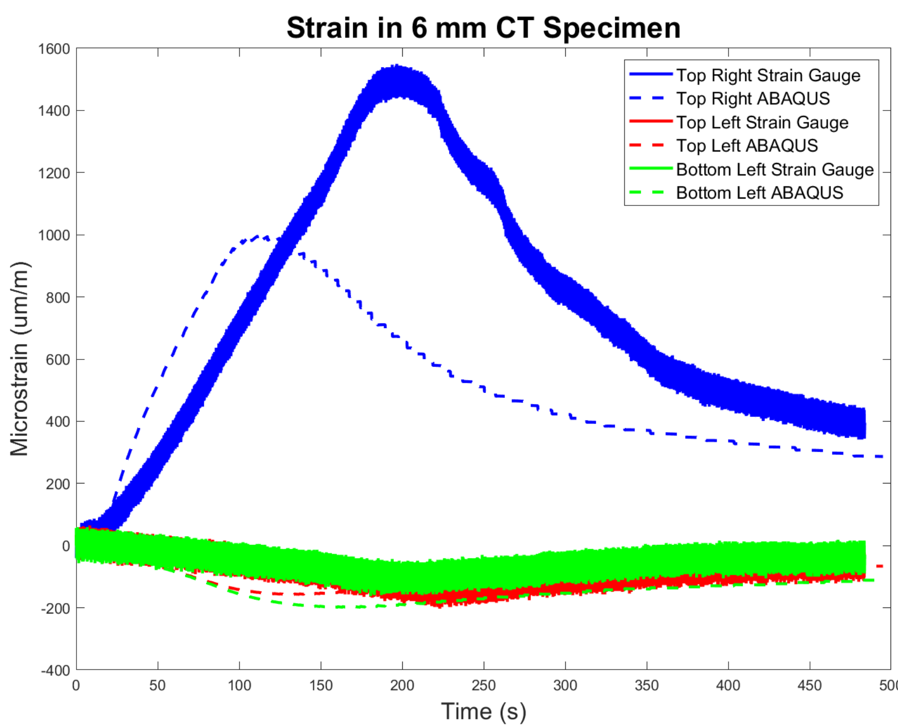

Figure A8: Time history of strain at three locations during failure due to fracture from strain gauge data vs elastic and elastic-plastic finite element models

It was found that both the top and bottom corners of the CT Specimen exhibit a strain of 150 microstrain which is well below the allowable value. The top left location was selected to create a sensor array like that shown during the PLB testing.

Appendix B: Supplemental Instrumentation Electronics

To accompany the testing of the NanoSonic USM strain sensors, three signal conditioning boards were used. These boards were designed by Josh Deem and the sensors group at NanoSonic in Pembroke, Virginia.

The first conditioning unit was used for the pencil lead break tests described in test 1 and 2 of the previous report. This 3-channel signal conditioning unit takes a resistance change from the USM sensor, and outputs a voltage. This is done by first balancing the USM sensor's resistance across a Wheatstone bridge. The bridge voltage is then amplified via a Texas Instruments INA849 high frequency amplifying chip. The unit features selectable gains of 50, 100, 200, and 500, with 500 being selected for the highlighted testing. The output of the amplifier is filtered via fourth order, dual op-amp filter of a frequency of 700 kHz to remove any extraneous noise to due environmental EMF and the switching frequency of the onboard power supply. A Texas Instruments ADA4022 chip was used for this filter. The board is capable of running 5-12V. The physical board is shown below in figure B1.

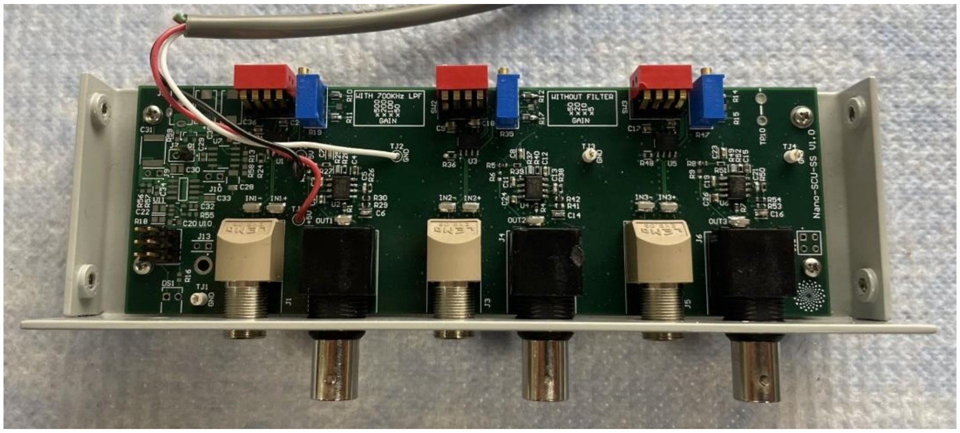

Figure B1: NanoSonic SCU for USM sensors

For the quasi-static fracture test two additional boards were implemented. A board was needed to amplify and filter the commercial Britek ultrasonic transducers. Amplification of the transducers was required due to the drastically lower levels of emissions that occur during crack propagation compared to the prior pencil lead break tests. In accordance with previous literature the transducers were amplified 40dB. The same Texas Instruments INA849 amplifier was used for this signal amplification. Additionally, to remove unwanted noise from the Instron a 5kHz highpass filter was used. A passive RC filter was selected using a 1 uF capacitor and a 330 ohm resistor in accordance with the cutoff frequency of an RC filter being

$$f = \frac{1}{2\pi RC} \tag{1}$$

The physical board is shown below in figure B2.

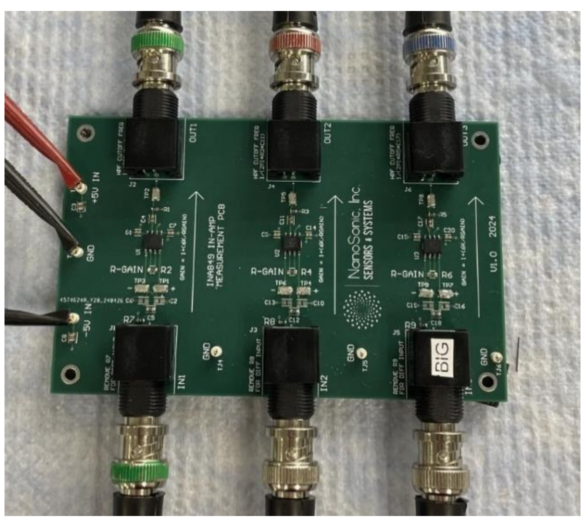

Figure B2: Amplification and filtering board for ultrasonic transducers

The final board used during the quasi-static fracture testing was a modified version of the signal conditioning unit mentioned above. This modified board only had two channels and sought to separate the high frequency, AC component data, from the low frequency, DC component. During the PLB testing this was done in post processing using the PicoScope data acquisition software. However, the resultant strain during fracture is significantly higher than that seen during the tensile PLB test. To obtain a good signal for source location in the AC term, a gain of at least 500 was required. This gain would cause the output rail to quickly saturate due to the large strain and voltage increase from the Wheatstone bridge. It was imperative that the DC and AC signals be amplified at separate rates. This division of signals was done by splitting the signal into two paths after the Wheatstone bridge and adding an RC high pass filter to one side. A pass frequency of 8 Hz was selected to remove the DC component as well as any additional low frequency noise. The modified board is shown below in figure B3.

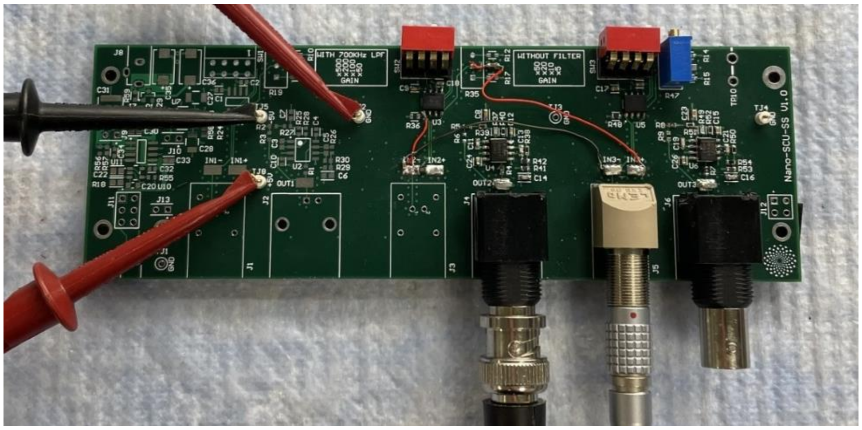

Figure B3: Modified SCU board to split signal for USM sensor